Plasma Sources Science and Technology

PAPER

Effect of negative gases admixture on the stability of beam-driven discharges

Plasma Sources Sci. Technol. **25** (2016) 064003 (7pp) doi:10.1088/0963-0252/25/6/064003

Effect of negative gases admixture on the stability of beam-driven discharges

Dmitry Levko and Laxminarayan L Raja

Department of Aerospace Engineering and Engineering Mechanics, The University of Texas at Austin, Austin, TX 78712, USA

E-mail: dima.levko@utexas.edu and lraja@mail.utexas.edu

Received 11 July 2016
Accepted for publication 16 September 2016
Published 14 October 2016

Abstract

The influence of negative gas SF_6 admixture on the stability of low-pressure beam-driven discharge is studied by self-consistent 1D particle-in-cell/Monte Carlo collisions model. We find that the plasma parameters as well as its stability are changed drastically when SF_6 is added to argon gas. In an electropositive plasma we obtain the excitation of both fast and slow electrostatic plasma waves which is explained by the propagation of electron beam through the non-homogeneous bounded plasma. These waves lead to the heating of plasma electrons and ions. On the other hand, in electronegative plasma we also obtain a decay of the electron beam. However, since in electronegative beam-generated plasma the electron plasma density is homogeneous the beam is more stable. As a consequence, we obtain only the excitation of two fast electrostatic waves. One wave is excited due to two-stream instability and another wave is excited due to beam decay. The excitation of these fast waves does not influence the plasma homogeneity but influences the heating of plasma electrons.

Keywords: beam-generated plasma, electronegative plasma, particle-in-cell

(Some figures may appear in colour only in the online journal)

1. Introduction

Beam-generated plasmas are used in many applications such as in surface modification [1], microwaves generation [2], thermal energy conversion devices [3] etc. Also, generation of plasma by high-energy electron beams has been proposed for use in next generation plasma processing technologies [4–6]. In the latter case, the use of electron beams allows for generation of large-area homogeneous plasma. Being a direct-current (dc) technology, beam-generated plasmas do not suffer from plasma non-uniformities as a consequence of non-uniformities in the electromagnetic wave power deposition as is typical in traditional inductively and capacitively coupled discharges [6]. Furthermore, the beam electron energy provides a readily controllable parameter for uniformity control.

It is known that the injection of electron beam into the low-density plasma can excite various types of instabilities [7, 8]. Moreover, the propagation of electron beam through neutralizing ion background bounded by the conducting walls can lead to the excitation of Pierce-type instability [8]. Recently, Kaganovich and Sydorenko studied the influence of boundaries on the two-stream instability [9]. They obtained that the instability growth rate γ depends on the distance between electrodes and beam velocity. Also, γ is a non-linear function of the electron plasma frequency. Moreover, γ is a linear function of the ratio between beam and plasma densities (n_b/n_p) unlike the case of an infinite plasma where $\gamma \propto (n_b/n_p)^{1/3}$. These facts must be taken into account during the development of plasma source because the excitation of this instability can significantly influence the heating of plasma electrons and plasma stability [10–12].

All cited results were obtained for electropositive plasma. However, electronegative plasmas are commonly used for materials etching applications and the properties of beam-generated plasma in electronegative gases must be studied [13]. A theoretical and experimental study of the beam-generated argon/SF_6 plasma in cylindrical tube was recently presented in [14]. In this work, a one-dimensional (1D) fluid simulation with drift-diffusion approximation was presented. The electron beam was treated as the additional ionization source term. The electron beam was collimated by an external axial magnetic field which allowed the plasma generation only near the source axis. The plasma generated at the axis then diffused along the tube radius making the problem 2D. The time scale of the heavy species diffusion is much longer than the source 'ignition' time. Moreover, since the electron beam is collimated by the axial magnetic field, the problem can be considered as the 1D during the stage of plasma generation.

In the present paper, we study the influence of the admixture of electronegative gas SF_6 to Ar on the chaotic behaviour of a beam-generated plasma studied in our previous paper [11]. In our study, we use 1D particle-in-cell/Monte Carlo collisions (PIC/MCC) model in which electron beam and plasma are generated self-consistently. Namely, electron beam is formed from the emitted electrons due to their acceleration in the high-voltage collisionless cathode sheath. Plasma is generated due to gas ionization by beam and plasma electrons.

2. Numerical model and initial conditions

The details of 1D PIC/MCC model used in our study are presented in [15]. Here, we describe only the additional processes added to this model.

In our previous paper [11], we studied the chaotic behavior of plasma generated by electrons emitted from the cathode due to thermionic emission. This effect was obtained for the emission current exceeding 20 A m^{-2}. Therefore, in the present study we fixed the emission current at $J_{em} = 40$ A m^{-2}. Electrons with the energy of 0.1 eV were injected in the cathode–anode (CA) gap in the vicinity of the cathode. Initially, the CA gap is plasma-free. The simulations are stopped when all plasma parameters reach a steady-state.

The CA gap is $d_{CA} = 5$ cm, the potential of the left boundary (cathode) is kept constant at $U_C = -100$ V, while the right boundary (anode) is grounded. Both boundaries are absorbing for electrons and ions. The background gas is the mixture of Ar and SF_6. The total gas pressure is 1 Pa, the gas is at room temperature (300 K).

The set of reactions considered in the model is shown in table 1. Reactions 1–5 are modeled using the method described, for instance, in [15]. Reaction #4 includes electronic excitation of Ar and electron momentum transfer reaction. Reaction #5 includes excitation of electronic and vibrational levels of SF_6 and electron momentum transfer reaction. Both reactions #4 and #5 are included only for the electron energy losses in inelastic collisions. In order to model the reactions #6–10, we, first, calculated the probability of each process. Then, we generated the random numbers in order to define the type of process that occurs. The probability of reactions #6–8 is calculated by $P_i = k_i n_g \cdot \Delta t$, where k_i is the rate coefficient of reaction, n_g is the background gas density, and Δt is the time step. The probability of momentum transfer reactions #9–10 is calculated by $P_i = \sigma n_g v_i \cdot \Delta t$, where $\sigma = \pi R^2$ is the cross section of Ar atom having radius R, and v_i is the particle velocity. The rate coefficients of reactions #6–8 are, respectively, $k_6 = 9 \times 10^{-16}$ m^3 s^{-1} and $k_{7,8} = 5 \times 10^{-14}$ m^3 s^{-1} [14].

Note that throughout this paper we distinguish between emitted electrons and electrons generated due to gas ionization.

Table 1. Reactions considered in 1D PIC/MCC model.

	Reaction	Type	Ref.
1	$Ar + e \rightarrow Ar^+ + 2e$	Ionization	[16]
2	$SF_6 + e \rightarrow SF_6^+ + 2e$	Ionization	[17]
3	$SF_6 + e \rightarrow SF_6^- + e$	Attachment	[17]
4	$Ar + e \rightarrow Ar + e$	Energy losses	[16]
5	$SF_6 + e \rightarrow SF_6 + e$	Energy losses	[17]
6	$Ar^+ + SF_6 \rightarrow Ar + SF_6^+$	Ion conversion	[14]
7	$Ar^+ + SF_6^- \rightarrow Ar + SF_6$	Recombination	[14]
8	$SF_6^+ + SF_6^- \rightarrow SF_6 + SF_6$	Recombination	[14]
9	$SF_6^+ + Ar \rightarrow SF_6^+ + Ar$	Mom. transfer	Based on radius
10	$Ar^+ + Ar \rightarrow Ar^+ + Ar$	Mom. transfer	

They are treated as the separate macro-particles having the same properties. The electrons generated due to gas ionization are called here the secondary (or plasma) electrons.

3. Theoretical analysis

In their paper [9], Kaganovich and Sydorenko studied the influence of boundaries on the two-stream instability of collisionless plasma. They obtained that the instability growth rate γ is the non-linear function of the plasma density (frequency), namely, γ increases faster that the linear function obtained for the infinite plasma. This allowed the authors to conclude that the presence of boundaries is responsible for the decay of fast Langmuir wave excited due to two-stream instability to slower waves. The interaction between plasma electrons and these slow waves was responsible for the acceleration of plasma electrons to the energies much larger that the plasma temperature (so-called supra-thermal electrons). This effect was also obtained in [11] for the plasma generated by a beam of thermo-emitted electrons in weakly collisional plasma.

We first analyze the steady-state spatial profiles of the plasma electrons density in electropositive and electronegative plasmas. We start with the electropositive plasma generated by the electron beam. For simplicity, we neglect the generation of plasma by plasma electrons. In the steady-state, the electron density profile is described by the equation:

$$\frac{d\Gamma_e}{dx} = k_i n_b n_g. \quad (1)$$

Here, k_i is the rate coefficient of gas ionization by electron beam with the density n_b, n_g is the background gas density, Γ_e is the flux of plasma electrons. In the drift-diffusion approximation which is valid at the considered conditions, the plasma species fluxes are

$$\Gamma_j = s_j \mu_j n_j E - \mu_j T_j \frac{dn_j}{dx}. \quad (2)$$

Here, E is the electric field strength, μ_j and T_j are the plasma species mobility and temperature, respectively. Species temperatures are assumed homogeneous for simplicity. Also, $s_j = 1$ for positive ions, and $s_j = -1$ for electrons and negative ions.

We neglect the beam flux in the total flux balance, i.e. assume rare beam-neutral collisions. Also, neglect the beam density in the quasineutrality condition, i.e. assume that the beam density is much smaller than the plasma density. Then, for electropositive plasma we obtain

$$\Gamma_e \approx -\mu_i T_e \frac{dn_e}{dx}. \tag{3}$$

In deriving this equation, we took into account that $\mu_e \gg \mu_i$ and $\mu_e T_e \gg \mu_i T_i$. Substituting equation (3) in equation (1), we find the equation for the electron density profile:

$$\frac{d^2 n_e}{dx^2} = -\frac{k_i n_b n_g}{\mu_i T_e}. \tag{4}$$

The right hand side of this equation is constant. The boundary conditions for this equation are

$$\frac{dn_e}{dx}(x=0) = 0,$$
$$n_e(x=0) = n_{e0},$$
$$n_e(x=l) = 0. \tag{5}$$

Here we assumed that point $x = 0$ corresponds to the center of the CA gap and $l = \frac{1}{2}d_{CA}$. Also, n_{e0} is the electron density in the center of the CA.

Using boundary conditions (5), we find from equation (4) the electron density profile:

$$n_e(x) = \frac{k_i n_b n_g}{2\mu_i T_e}(l^2 - x^2). \tag{6}$$

We see that the peak density of plasma electrons is $n_{e,0} = \frac{k_i n_b n_g}{2\mu_i T_e} l^2$, i.e. it is proportional to the beam density. Equation (6) means that the electron plasma frequency is a linear function of position.

Now, let us consider the electronegative plasma. We neglect again the contribution of electron beam into the flux balance and quasineutrality. Electron attachment cross section for beam electrons is much smaller than that for plasma electrons. Then, taking into account that $\mu_e \gg \mu_i$ and $\mu_e T_e \gg \mu_i T_i$, we find the electron flux:

$$\Gamma_e \approx -\frac{2\mu_e \mu_i T_e n_n dn_e/dx}{\mu_e n_e + 2\mu_i n_n}. \tag{7}$$

Here, n_n is the negative ion density. This equation shows that depending on the ratio $\mu_e n_e/(2\mu_i n_n)$ two different regimes are possible. In the first regime, $\mu_e n_e \gg 2\mu_i n_n$, i.e. in the case of low electronegativity plasma electron density equation is nonlinear and it is difficult to analyze analytically. However, in this paper, we are interested in the regime of highly electronegative plasma for which $\mu_e n_e \ll 2\mu_i n_p$ (see discussion in section 5). Then, the flux (7) is simplified as

$$\Gamma_e \approx -\mu_e T_e \frac{dn_e}{dx} \tag{8}$$

and equation for the electron density profile is written as

$$\frac{d^2 n_e}{dx^2} - \frac{k_a n_g}{\mu_e T_e} n_e = -\frac{k_i n_b n_g}{\mu_e T_e}. \tag{9}$$

This is the linear equation which can be solved analytically. The boundary conditions for equation (9) are defined by (5). In equation (9), we took into account the attachment of plasma electrons to the electronegative gas (see discussion below). This process is described by the rate coefficient k_a. The attachment of beam electrons can be neglected because k_a is negligibly small for electron energy ~100 eV.

The general solution of equation (9) is

$$n_e(x) = Ae^{-kx} + Be^{kx} + C,$$

where A, B, C and k are constants. Using boundary conditions, we find $k^2 = \frac{k_a n_g}{\mu_e T_e}$, $A = B = \frac{k_i n_b n_g}{\mu_e T_e (e^{-kl} + e^{kl})}$. Thus, the solution of equation (9) is

$$n_e(x) = -\frac{k_i n_b}{k_a}\frac{e^{-kx} + e^{kx}}{e^{-kl} + e^{kl}} + \frac{k_i n_b}{k_a}. \tag{10}$$

Using typical values $k_a \sim 10^{-15}$ m^3 s^{-1}, $n_g \sim 10^{20}$ m^{-3}, $\mu_e \sim 10^4$ m^2 V^{-1} s^{-1} and $T_e \sim 1$ eV we estimate $k \sim 3.2$ m^{-1} and $kl \sim 0.16$. Thus, function $\frac{e^{-kx} + e^{kx}}{e^{-kl} + e^{kl}}$ does not depend significantly on x and electron density in electronegative beam-generated plasma can be approximated by

$$n_e(x) \approx \frac{k_i n_b}{k_a} c, \tag{11}$$

where c is some small constant.

Thus, we conclude that in electropositive beam-generated plasma the electron plasma frequency increases toward the center of the CA gap as the linear function of position. Hence, the instability growth rate also increases toward the center. At the same time, in the electronegative beam-generated plasma the electron plasma frequency is almost constant. This means that the growth rate of two-stream instability does not depend on the beam position.

4. Electropositive plasma

Now, let us discuss the results of 1D PIC/MCC simulations obtained for $J_{em} = 40$ A m^{-2}. First, we start with the results obtained for the electropositive electron/Ar$^+$ plasma (figures 1–3). These results are similar with those presented in our previous paper [11] for high beam current density. Therefore, we discuss only on the main points about this case.

Emitted electrons lead to the formation of plasma having density $n_e \sim 10^{10}$ cm^{-3} (figure 1(b)). This density is enough to screen the applied electric field (figure 1(a)) leading to the formation of the narrow sheath in the vicinity of the cathode. This sheath is collisionless for emitted electrons. Therefore, these electrons are accelerated in the sheath leading to the beam formation (beam energy ~ 120 eV). This beam is the main source of plasma in the CA gap.

Figure 1(a) shows electric field obtained at three instants of time. We see the propagation of waves from the cathode to the anode. The amplitude of these waves varies in the CA gap reaching its maximum near the center of the gap where the peak plasma density is obtained (figure 1(b)). Then, the amplitude of these waves decreases toward the anode where

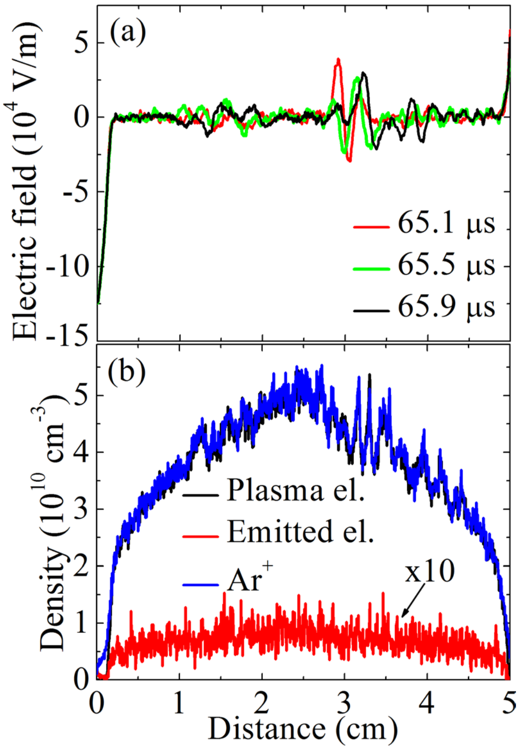

Figure 1. (a) Electric field and (b) plasma species densities obtained in electropositive plasma.

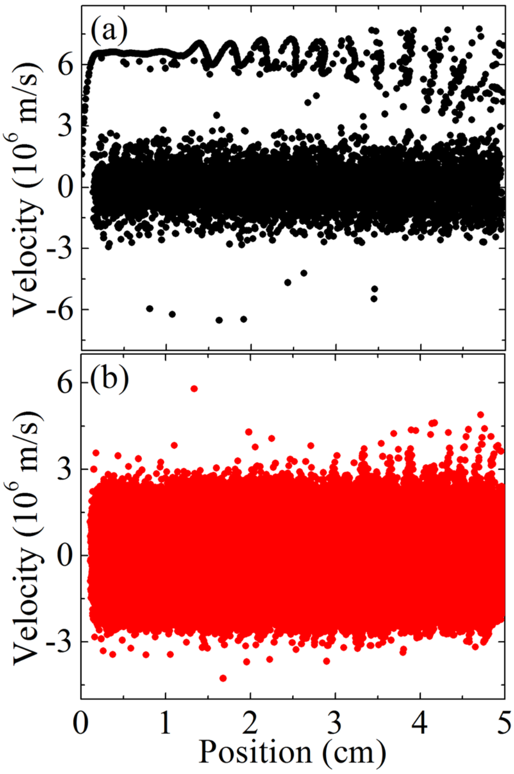

Figure 2. Phase space of (a) emitted electrons and (b) plasma electrons obtained in electropositive plasma at $t = 65.9\ \mu$s.

the plasma density decreases. The instability growth rate in bounded plasma is defined as [9]

$$\gamma \approx \left(\frac{1}{13}\right)\omega_{pe}\alpha\left(d_{CA}\omega_{pe}/v_b\right)\ln\left(d_{CA}\omega_{pe}/v_b\right) \times\left[1-0.18\ \cos\left(d_{CA}\omega_{pe}/v_b+\pi/2\right)\right]. \quad (12)$$

It is the largest in the location where the plasma density is the largest (ω_{pe} is the electron plasma frequency).

The phase space of emitted and plasma electrons are shown in figure 2. Figure 2(a) shows the disruption of the electron beam. Namely, one can see almost monoenergetic beam only along the first centimeter. At larger distance the beam energy starts oscillating and near the center of the CA gap the beam completely losses its stability. Figure 2(a) shows that there is no beam in the right half of the simulation domain. The mean free path of the electron beam in argon gas at 1 Pa is estimated as $\lambda = \frac{1}{[n_g\sigma(120\,\text{eV})]} \sim 7$ cm, i.e. it exceeds d_{CA}. Thus, the beam decay is only explained by the interaction between beam and electrostatic waves excited by this beam. The approximate expression for the spatial growth rate is [9]

$$\text{Im}(k) \approx \frac{2\cdot\ln\left(\frac{\omega_{pe}d_{CA}}{v_b}\right)-0.5}{d_{CA}}. \quad (13)$$

Here, k is the wave number. Substituting $v_b = 6\times10^6$ m s^{-1} (figure 2(a)), $n_e = 10^{10}$ cm^{-3} (figure 1(b)), we find $\text{Im}(k) \approx 1.4\times10^2$ m^{-1}, i.e. the length scale of the instability growth is estimated as $1/\text{Im}(k) \approx 0.7$ cm which agrees with the results shown in figures 1–2.

Figure 2(b) shows the generation of supra-thermal plasma electrons in the right half of the CA gap. The mechanism of generation of these electrons is presented in [10, 11]. Here, we recall the main details of this mechanism.

The propagation of the electron beam through the bounded plasma excites two-stream instability. This wave is unstable due to non-homogeneous profile of the plasma density and consequent non-linear dependence of the instability growth rate. Thus, the wave decays into several waves having smaller phase velocities and having wavelengths shorter than the wavelength of primary wave. Waves having small phase velocities are in resonance with the plasma electrons. Therefore, the resonant interaction between electrostatic waves and plasma electrons becomes possible. This interaction is responsible for the heating of plasma electrons and for the generation of supra-thermal electrons (see figure 2(b)).

The electric field in the center of the CA gap and its Fourier spectrum are shown in figures 3(a) and (b), respectively. We see the irregular oscillations of electric field whose amplitude reaches ~10^4 V m^{-1}. Figure 3(b) shows the excitation of strong harmonics of electric field having ion plasma frequency ($\omega_{p,i} \approx 20$ MHz) and smaller. These low-frequency waves having small phase velocity cause the heating of plasma ions leading to the modification of the ion density profile. Indeed, figure 1(b) shows sharp oscillations of the ion density profile in the right half of the CA gap.

5. Electronegative plasma

We now analyze the results obtained for the Ar/SF_6 mixture (90% of argon). We note that we were unable to initiate the discharge for $U_C = -100$ V and $J_{em} = 40$ A m^{-2} for cases with more than 80% of SF_6 in the mixture. The results of

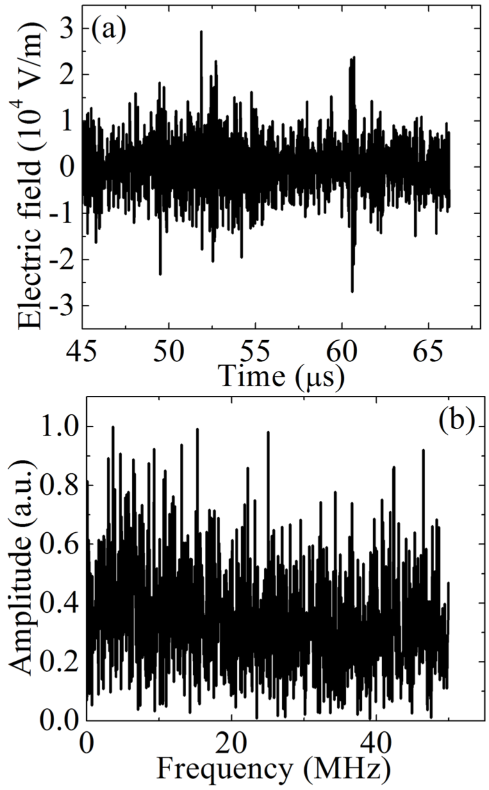

Figure 3. (a) Time evolution of electric field in the center of the cathode–anode gap, and (b) Fourier spectrum of this electric field.

simulations are shown in figures 4–7. We conclude that the admixture of SF_6 changes drastically the plasma parameters and its dynamics.

Figure 4(b) shows that the dominant negative species in the plasma are ions SF_6^-. These species are mainly generated due to attachment of plasma electrons to SF_6. The attachment of beam electrons to SF_6 is negligibly small due to small electron attachment cross section at 120 eV. The densities of positive ions SF_6^+ and Ar^+ are comparable in spite of the much larger density of Ar in comparison with the density of SF_6. This result is in qualitative agreement with the recent observations for the beam-generated Ar/SF_6 plasma [14]. It is explained by the conversion of Ar^+ to SF_6^+ in reaction #6 (table 1).

Our simulation results have shown that ~30% of Ar^+ ions are generated by plasma electrons and ~70% are generated by emitted electrons. At the same time, ~5% of SF_6^+ are generated by plasma electrons, ~30% by emitted electrons and ~65% due to the ion conversion reaction #6 (table 1).

It is interesting to note that the spatial structure of the beam-generated electronegative plasma is similar with that obtained in homogeneous external magnetic field with magnetized electrons and unmagnetized ions [18]. Namely, there is no positive–negative ion core and electron/positive ion sheath which is usually obtained in unmagnetized electronegative plasma [13]. Instead, we see in figure 4 highly electronegative plasma (n_n/n_e ~ 100) throughout the CA gap (see discussion in section 3).

In order to understand the plasma dynamics, we use the discussion presented in section 3. At the considered conditions, the mobility of plasma electrons is estimated as $\mu_e = \frac{q_e}{m_e v_{th} n_g \sigma_m} \approx 7.3 \times 10^3\,m^2\,V^{-1}\,s^{-1}$. Here, q_e is the elementary charge, m_e is the electron mass, $\sigma_m \sim 10^{-19}\,m^2$ is the electron momentum cross section taken for electrons in Ar gas. Also, we substituted $v_{th} \sim 10^6\,m\,s^{-1}$. In analogy, the mobility of Ar^+ is estimated as $\mu_i \approx 2.7 \times 10^2\,m^2\,V^{-1}\,s^{-1}$. Figure 4 shows the electron density $n_e \sim 10^9\,cm^{-3}$ and ion density $n_p \sim 10^{11}\,cm^{-3}$. Thus, $\frac{\mu_e n_e}{2\mu_i n_p} \approx 0.1 \ll 1$ which means that the approximation (8) for electron flux in beam-generated plasma is valid. Then, the density of plasma electrons is defined by equation (11), i.e. it is almost homogeneous throughout the CA gap. This result agrees with the results shown in figure 4(c).

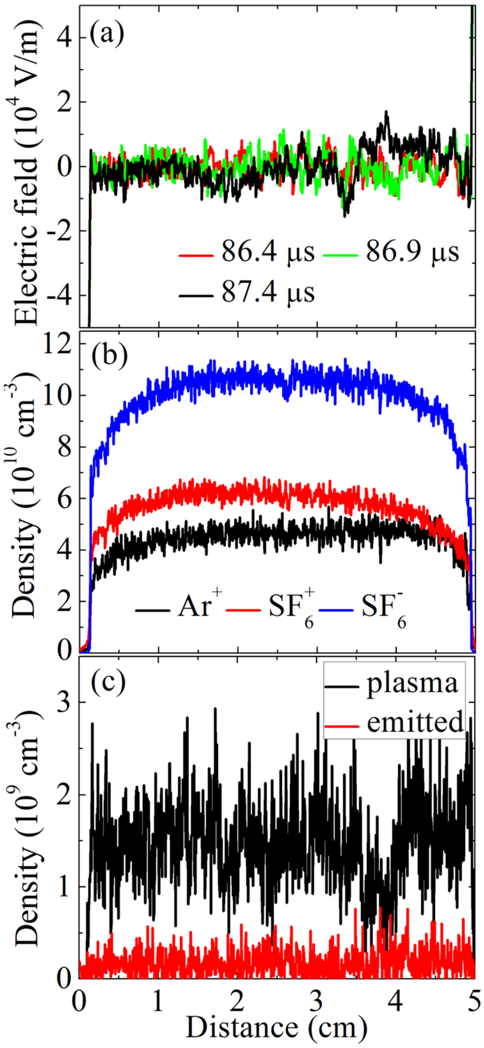

Figure 4. (a) Electric field, (b) ion densities, and (c) plasma and emitted electrons densities obtained in electronegative plasma.

Thus, the profile of electron plasma density in beam-generated electronegative plasma is homogeneous unlike in the case of electropositive plasma, where the electron density profile is the square function of the distance from the electrodes (see equation (6) and figure 1(b)). This means that the electron plasma frequency does not depend on position. As a consequence, the instability growth rate [9] does not depend on position as well. Moreover, the peak of electron plasma density in electronegative plasma is ~2 orders of magnitude smaller than that in electropositive plasma (compare

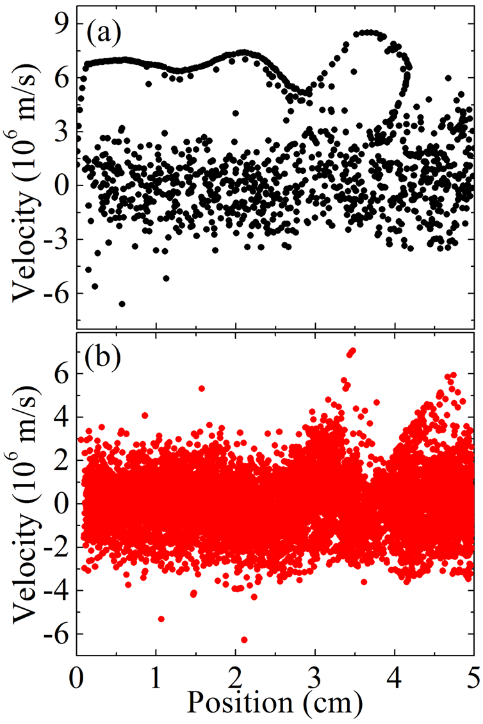

Figure 5. Phase space of (a) emitted and (b) plasma electrons obtained in electronegative plasma at $t = 87.4$ μs.

figures 1(b) and 4(c)). This results in smaller instability growth rate in electronegative plasma.

Figure 5(a) shows the disruption of the electron beam in spite of almost homogeneous density of plasma electrons. Moreover, figure 5(a) shows that large fraction of emitted electrons entering the plasma bulk as the electron beam dissipates all its energy. The beam disruption as it follows from figure 5(b) leads again to the generation of supra-thermal plasma electrons. In order to understand this beam dynamics we analyze the time evolution of electric field shown in figure 6(a) and its Fourier spectrum shown in figure 6(b). One can see the excitation of electrostatic wave having frequency ~10 MHz. This wave is excited by two-stream electron instability. Also, we obtain from figure 6(b) the generation of higher harmonic (frequency ~40 MHz) having smaller amplitude. The insert shown in figure 6(b) shows the Fourier spectrum of electric field obtained at the distance of $0.25 \times d_{CA}$. The comparison between this spectrum and spectrum obtained in the center of the gap allows us to conclude that the generation of higher harmonic is caused by the beam disruption.

Thus, the propagation of electron beam through the electronegative plasma is accompanied by the excitation of two-stream instability. Using equation (12) and plasma parameters shown in figure 4 (α ~ 0.005) we obtain γ ~ 20 MHz which agrees with the frequency of higher harmonic seen in figure 6(b). The phase velocity of this instability is of the order of magnitude of the beam velocity, i.e. the interaction between excited wave and plasma electrons is impossible. However, this wave interacts with the beam electrons (Landau damping [8]) leading to their deceleration/acceleration (figure 5(a)).

The dependence of the instability growth rate (12) on beam velocity for fixed electron plasma density ($\approx 10^9$ cm^{-3}) and

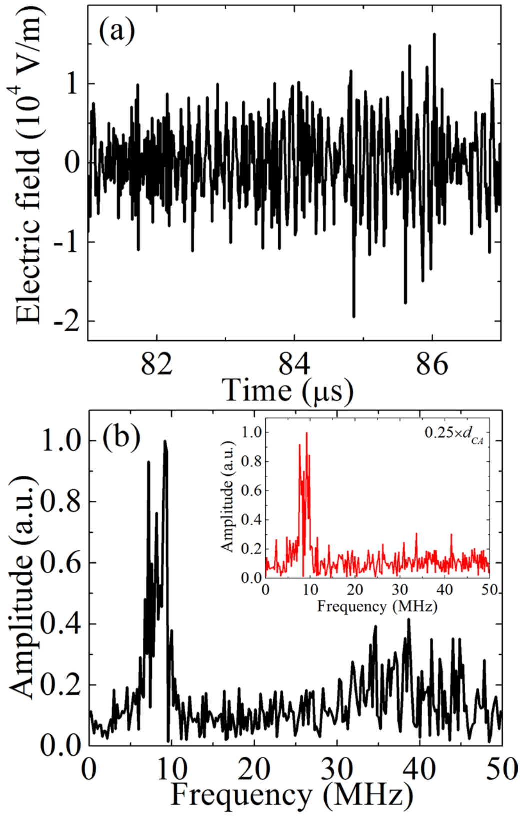

Figure 6. (a) Time evolution of electric field in the center of the cathode–anode gap, and (b) Fourier spectrum of this electric field; insert in figure (b) shows the Fourier spectrum of electric field at the distance of $0.25 \times d_{CA}$.

α ~ 0.005 is shown in figure 7. One can see that γ is the non-linear function of v_b in the range 5×10^6 m s^{-1} $< v_b < 7 \times 10^6$ m s^{-1} (see figure 5(a)). We conclude that the beam deceleration due to its interaction with electrostatic wave leads to the increase of γ. This destabilizes the electron beam leading to its decay near the anode (figure 5(a)). Since the decrease in the beam velocity leads to the increase in the γ the deceleration of the electron beam leads to the excitation of wave having higher frequency (figure 6(b)). Substituting in equation (12) $v_b \approx 3 \times 10^6$ m s^{-1} we find Im(k) $\approx$ 125 m^{-1}. Then, the phase velocity of the higher harmonic with $\nu \approx 40$ MHz is estimated as v_{ph} ~ ν/Im(k) ~ 3×10^5 m s^{-1}. This wave can interact with plasma electrons leading to their heating up to supra-thermal energies (figure 5(b)). Also, it is important to note from figures 4(c) and 5(b) that the acceleration of plasma electrons makes local electron plasma density non-homogeneous. As a consequence, the dependence of the instability growth rate on the local electron plasma frequency starts playing a role.

Figure 4(b) allows us to conclude that the ion density remains almost homogeneous in spite of the instability of the electron beam. This is explained by the fact that in electronegative plasma only fast waves are excited (figure 6(b)). The phase velocity of these waves is much larger than the ion thermal velocity. Therefore, the resonant ion-wave interaction is impossible in this plasma. However, the beam decay is important for the generation of rather dense electronegative plasma because it leads to the heating of plasma electrons.

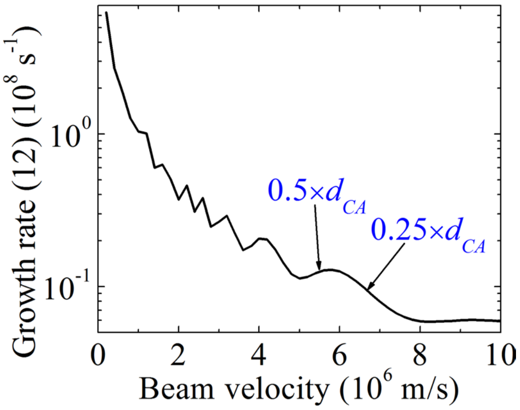

Figure 7. Influence of the beam velocity on the instability growth rate (12) for the plasma parameters shown in figure 1.

Also, dissipation of beam energy leads to the population of plasma by energetic electrons (figure 4(a)). Our simulation results have shown that ~60% of plasma is generated by emitted electrons from Ar, ~18% is generated by emitted electrons from SF_6, and ~18% and ~4% is generated by plasma electrons from Ar and SF_6, respectively.

6. Conclusions

The influence of electronegative gas SF_6 on the low-pressure plasma instability is studied using a 1D particle-in-cell/Monte Carlo collisions model. The plasma was generated by the electron beam which is generated from the electrons emitted from the cathode and accelerated in the collisionless cathode sheath.

We obtained that the small impurity of SF_6 influences significantly the plasma stabilization. This was explained by the significantly different profile of the electron density generated by the electron beam in electropositive and electronegative plasmas. Namely, in electropositive plasma the electron density profile was a square function of the position while in the electronegative plasma it was homogeneous. As a consequence, the instability growth rate was a strong function of position in the electropositive plasma and did not depend on position in electronegative plasma. In addition, the electron plasma frequency was much smaller in electronegative plasma due to the electron attachment to SF_6 and formation of heavy negative ions.

However, we obtained the deceleration of the electron beam in electronegative plasma in spite of the homogeneous electron plasma frequency. This was explained by the interaction between electron beam and electrostatic wave excited due to two-stream instability. This interaction led to the deceleration of the beam electrons and, as a consequence, led to the increase of the local instability growth rate.

References

[1] An W, Krasik Ya E, Fetzer R, Bazylev B, Mueller G, Weisenburger A and Bernshtam V 2011 *J. Appl. Phys.* **110** 093304
[2] Benford J, Swegle J A and Schamiloglu E 2007 *High Power Microwaves* 2nd edn (London: Taylor and Francis)
[3] Hatsopoulos G N and Gyfopoulos E P 1973 *Thermionic Energy Conversion* (Cambridge, MA: MIT Press)
[4] Dorf L, Rauf S, Collins K S, Misra N, Carducci J D, Leray G and Ramaswamy K 2015 *US Patent* #US 8,951,384 B2
[5] Petrov G M, Boris D R, Petrova Tz B, Lock E H, Fernsler R F and Walton S G 2013 *Plasma Sources Sci. Technol.* **22** 065005
[6] Samukawa S *et al* 2012 *J. Phys. D: Appl. Phys.* **45** 253001
[7] Mikhailovkii A B 1975 *Theory of Plasma Instabilities* vol 1 (Moscow: Atomizdat)
[8] Nezlin M V 1993 *Physics of Intense Beams in Plasmas* (Boca Raton, FL: CRC Press)
[9] Kaganovich I D and Sydorenko D (arXiv:1503.04695)
[10] Sydorenko D, Kaganovich I D, Chen L and Ventzek P L G 2015 *Phys. Plasmas* **22** 123510
[11] Levko D and Raja L L 2016 *Phys. Plasmas* **23** 032107
[12] Morey I J and Boswell R W 1989 *Phys. Fluids* B **1** 1502
[13] Lieberman M A and Lichtenberg A J 2005 *Principles of Plasma Discharges and Materials Processing* (New York: Wiley)
[14] Petrov G M, Boris D R, Petrova T B and Walton S G 2016 *J. Vac. Sci. Technol.* A **34** 021302
[15] Levko D 2013 *J. Appl. Phys.* **114** 223302
[16] Yamabe C, Buckman S J and Phelps A V 1983 *Phys. Rev.* A **27** 1345
[17] Christophorou L G and Olthoff J K 2000 *J. Phys. Chem. Ref. Data* **29** 267
[18] Levko D, Garrigues L and Hagelaar G J M 2014 *J. Phys. D: Appl. Phys.* **47** 045205